Time-variable 3D ground displacements from High-Resolution Synthetic Aperture Radar (SAR). Application to La Valette landslide (South French Alps).

Daniel Raucoules, Marcello De Michele, Jean-Philippe Malet, Patrice Ulrich

Time-variable 3D ground displacements from High-Resolution Synthetic Aperture Radar (SAR). Application to La Valette landslide (South French Alps).

Raucoules D.[1*], de Michele M.[1], Malet J.-P.[2], Ulrich P. [2]

1. BRGM, Bureau de Recherches Géologiques et Minières, 3 Avenue Claude Guillemin, F-45060 Orléans, France.
2. Institut de Physique du Globe de Strasbourg, CNRS UMR 7516, EOST / Université de Strasbourg, 5 rue Descartes, F-67084 Strasbourg Cedex, France.

* corresponding author, email: d.raucoules@brgm.fr

Abstract

We apply an image correlation technique to multi-orbit and multi-temporal High-Resolution (HR) SAR data. Image correlation technique has the advantage of providing displacement maps in two directions; e.g. the Line of Sight direction (LoS) and the Azimuth direction. This information, derived from the two modes of data acquisition (ascending and descending), can be combined routinely to infer the three dimensional surface displacement field at different epochs. In this study, a methodology is developed to characterize the displacement pattern of the large La Valette landslide (South French Alps) using TerraSAR-X images acquired in 2010. The results allow mapping the dynamics of different units of the La Valette landslide at high spatial resolution. The study demonstrates the potential of this new application of High Resolution SAR image correlation technique for landslide ground surface deformation monitoring.

Introduction

Slope movements such as landslides are one of the most significant geo-hazards in terms of socio-economic costs. Displacement monitoring of unstable slopes is thus crucial for the prevention and the forecast. In areas where large landslides cannot be stabilized and may accelerate suddenly, remote monitoring is often the only solution for surveying and early-warning. The choice of an adequate monitoring system depends on several constraints such as the landslide type, the areal extension, the

range of observed velocity, the frequency of data acquisition, the desired accuracy and by the cost of data acquisition and processing. Techniques based on High Resolution (HR) Space-borne SAR could provide valuable information in terms of landslide monitoring. In this framework, the availability of HR SAR such as the German Space Agency (DLR) Terrasar-X (TSX) data with frequent repeat cycle (11 days) represents an opportunity for constructing frequent landslide displacement maps in the perspective of an operational use.

The sub-pixel correlation technique is based on the measurement of sub-pixel offsets between SAR images acquired at different dates. The method is based on a local correlation analysis that can be performed in the Fourier domain (as is presented in the current study) or in the spatial domain (e.g. Delacourt et al., 2004). Once the SAR data are perfectly co-registered, lines and columns (e.g. azimuth and range directions) offsets between two SAR data are converted in surface displacement estimates (e.g. Michel & Avouac, 2002; de Michele et al., 2010). Typically, the precision of the technique can reach about 1/10 of a pixel or even more (e. g. Leprince et al., 2007) depending both on the characteristics of the data (acquisition geometry, changes that occurred between the acquisitions, instrumental noise) and the amplitude of ground displacement (e.g. notably its spatial wavelength with respect to the size of the correlation window). This technique has been successfully applied to optical and radar data for studying deformation patterns originated from earthquakes (e.g. Michel and Avouac, 2002; de Michele et al., 2010), glacier kinematics (e.g. Scambos et al., 1992; Wangensteen et al., 2006) and landslides (Delacourt et al., 2009; Travelletti et al., 2012a). However, in regions characterized by the presence of persistent cloud cover, passive sensor data have important limitations preventing the creation of reliable archives of images for long-term monitoring. Data from active sensors such as HR SAR amplitude can be an alternative to optical imagery. The primary interests of using such data are threefold. First, the SAR amplitude is little or even not affected by the cloud cover or the atmospheric disturbances compared to SAR interferometry (InSAR). Second, the backscatter amplitude is less affected by multi-temporal vegetation changes than the phase of the signal commonly used in InSAR. Third, SAR amplitude is not affected by signal saturation in the presence of high displacement gradient.

Ionospheric disturbances could, in specific cases (e.g. Quegan & Lamont, 1986), produce anomalous signatures on the azimuth offset estimations due to azimuth misregistration errors of the processed images. As the ionosphere is a dispersive medium for microwaves, such an effect mainly concerns the

radar data obtained by sensors based on longer wavelength (e.g. L-band sensors). It is thus assumed that results derived from X-band data are little disturbed by the ionosphere except for the geographic locations that are affected by very high Total Electron Content (such as the polar regions; Mattar & Gray, 2002). It has been shown that *a posteriori* comparison of several azimuth offset maps allows detecting and rejecting offset results affected by ionospheric disturbances (e.g. Raucoules & de Michele, 2010).

A further advantage of using SAR imagery is the high attitude control of the platform, which provides very similar geometrical conditions for image acquisitions (e.g perpendicular baselines generally shorter than few hundreds of metres). In such conditions, where the Base to Height ratio (B/H) ~ 10^{-3}, the topographic contribution to the range offsets is rather moderate (for 1m pixel size, a 100 m height variation would correspond to about 0.1 pixel). By selecting smaller baselines, the topographic component can even be decreased (in the presence of steep relief, for instance) and in several cases, as the presented one, there is no need to correct the topographic component.

With this basis, the ability of TSX (as well as other HR SAR sensors) of providing amplitude images with resolution equivalent to optical remote sensing data (~1m) is of major interest. Given the high spatial resolution of the TSX data, displacements fields in the azimuth and range directions can be measured with an expected precision of about 0.1 m at different acquisition dates.

The objectives of this work are threefold. First, we intend to evaluate the capability of the SAR amplitude offset technique to obtain landslide displacement maps with TSX data. Second, we explore the possibility of combining offsets maps into time series using least-square approaches (Usai, 2003; Le Mouelic et al., 2005; Casu et al., 2011). Third, we intend to combine ascending and descending modes to retrieve the multi-temporal 3D surface displacement fields,. The study could be of particular interest for detecting changes in surface displacement rates (e.g. acceleration and deceleration) at high spatial resolution. This could help for the forecast of large movements. To reach the aforementioned goals, we have decided to plan the acquisitions of TSX Spotlight data (1m resolution) at La Valette landslide (South French Alps) during one year, from April 2010 to March 2011. This landslide is characterized by displacement rates of about a dam/yr (e.g. Colas & Locat, 1992; Travelletti et al., 2012b). Eight TSX Spotlight data in ascending mode and thirteen in descending mode have been acquired.

Geological setting and history of the landslide

The La Valette landslide is one of the largest and more complex slope movement in the South French Alps, and has been triggered in March 1982. The landslide features two styles of behaviors; a translational slide type with the development of a flow tongue in the medium and lower part, and a slump-type with the development of multiple rotational slides in the upper part at the main scarp. The landslide extends over a length of 2 km. It features a variable width ranging from 0.2 km in the lower and medium parts to 0.4 m in the upper part. The maximum depth, estimated by seismic and electrical resistivity tomography and geotechnical boreholes, varies from 25 m in the lower and middle parts (e.g. Travelletti et al., 2009; Hibert et al., 2012; Samyn et al., 2012) to 35 m in the upper part (Le Mignon, 2004; Travelletti et al., 2012b). The mean slope gradient is ca. 30° in the scarp area and ca. 20° in the translational slide area. The volume of the landslide is estimated at 3.5 10^6 m^3.

The landslide affects a hill slope located uphill of the municipality of St-Pons (Alpes-de-Haute-Provence Department). It represents a significant threat for the 170 community housings located downhill (Le Mignon & Cojean, 2002). The occurrence of rapid mudflows triggered in the scarp area in the 1980s and 1990s has motivated the development of an early-warning system since 1991 composed of benchmark topographical monitoring, optical and infra-red camera monitoring and the installation debris height detection sensors in the torrent, and the drainage of the lower part of the landslide.

The landslide exhibits a complex style of activity in space and time. It has developed first as a rotational slide affecting the Autapie sheet thrust in relation to a major fault system (Colas & Locat 1993). The failed mass has progressively loaded the underlying black marls formation, and the landslide has progressed downhill by a series of rapid mudflows triggered in the marls such as in March 1982, April 1988, March 1989 and March 1992. The most important acceleration occurred in 1988 when a mudflow of 50.000 m^3 triggered at the elevation of 1400 m over a distance of ca. 500 m. For the moment, these mudflows did not generate a cascade mobilization of the entire landslide mass.

The ground displacements are monitored permanently with topometric benchmarks since 1991 (Squarzoni et al. 2005), differential dual-frequency GPS (Malet et al., 2012) and an extensometer since 2008. At regular periods the monitoring is performed also by digital correlation of terrestrial photos (Travelletti et al., 2012) and satellite radar interferometry (Squarzoni et al. 2003). Two main aspects can be pointed out from these past monitoring studies and from the observations by the local

risk managers. First, they observed a decrease of velocity (from 0.4 m.day^{-1} to about 0.01 m.day^{-1}) in the middle and lower part of the landslide caused by the local groundwater drawdown since the installation of a drainage system in the 1990s. Second, they pointed out an important activity of the upper part at the Soleil Boeuf crest since year 2000. This activity is characterized by a rapid retrogression of the main scarp towards the North-East and an enlargement of the landslide towards the North-West. In response to this worrying situation, the RTM Service has installed several additional benchmarks along profiles both in the unstable and stable parts of the Soleil-Boeuf crest to monitor the displacements in the crown area. Actually, an accumulation of material and a steepening of the slope are observed in the upper part because of the retrogression of the scarp (Travelletti et al., 2012b). Consequently, the possible hazard scenario consists in the untrained loading of underlying black marls formation and the triggering of new rapid and mobile mudflows.

High resolution radar dataset

The Table 1 lists the TSX spotlight images used for the analysis. The objective of the satellite programmation was to obtain a sufficient amount of data to estimate the changes in displacement rates during the study period. Thus the image acquisition rate has been deliberately increased for the periods between March and June as changes in the displacement regime (due to possible changes in the sub-surface water circulation in spring) were expected.

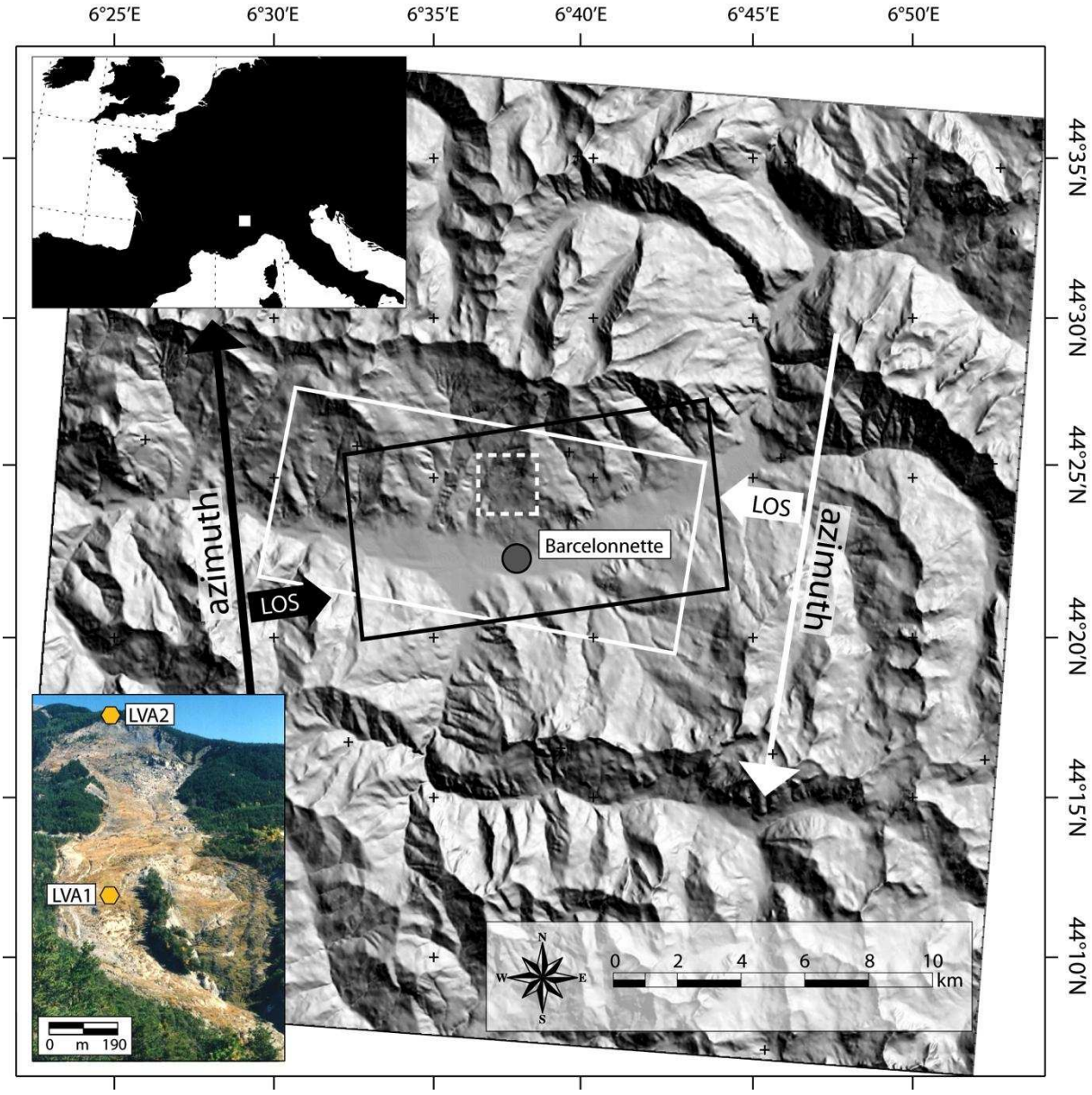

Figure 1: The Barcelonnette area of interest in the South French Alps. The white dotted line corresponds the location of the La Valette landslide and to the frame of Figures 2 and 3. The extension of the TSX acquisition frames are indicated in white (descending mode) and black (ascending mode). The bottom right terrestrial photograph presents the morphology of the landslide in 2009.

The ascending data set is incomplete due to failure in the data acquisition. However, the period between April and November 2010 is globally well covered. We preferred to plan data acquisitions with incidence angles of 41°.2 (ascending mode) and 49°.3 (descending mode) in order to minimize the surface affected by lay-over and shadowing phenomena.

Table 1. TerraSAR-X HR spotlight data acquired for the analysis.

Month	Ascending	Descending
April 2010	2010-04-08	2010-04-04
May 2010	2010-05-11	2010-05-18
	2010-05-22	
June 2010	2010-06-02	2010-06-09
	2010-06-13	2010-06-20
July 2010	2010-07-05	2010-07-01
August 2010	2010-08-07	
September 2010		
October 2010		2010-10-08
November 2010	2010-11-03	2010-11-10
December 2010		2010-12-13
January 2011		2011-01-15
February 2011		2011-02-06
March 2011		2011-03-11
		2011-03-22
April 2011		2011-04-13

Methodology

Sub-pixel image correlation

The objective is to estimate local changes in the position of elements at the ground surface by comparing two images acquired at different dates. The observed position change on the image is interpreted as displacement. The estimation of such offsets (both in azimuth and range directions) is obtained by local correlation processing on the image pair. The method applied to SAR amplitude images has been firstly described by Michel et al. (1999) and is today widely used in characterization of tectonic plate movement associated to earthquake (e.g. de Michele et al. 2010 or Pathier et al.

2005). For this study, the image correlator implemented in the GAMMA software has been used along with the "offset-tracking" procedure (Werner et al., 2005). This kind of technique is known to provide offsets estimation with a precision up to 1/20-1/10 pixel (and thus sometimes named sub-pixel correlation). Bamler & Eineder (2005) proposed a theoretical estimate of the error standard deviation for offsets derived from incoherent correlation methods (Eq. 1):

$$\sigma \sim \sqrt{\frac{3}{N}} \frac{\sqrt{1-\gamma^2}}{\pi\gamma} \quad (1)$$

where γ is the coherence value and N is the number of pixels within the estimation window.

The GAMMA software offset-tracking procedure provides SNR estimations for each offset by comparing the height of the correlation peak relative to the average level of the correlation function. They are indicators of the confidence in offsets estimates. The average of resulting SNR values on the landslide is higher than 11 suggesting high coherence levels. The connection between SNR values produced by the correlation tool and coherence is not straightforward (Wegmuller, personal communication) but, we such high SNR values, we can expect coherence values ranging at least between 0.8 and 0.9. Using estimation window sizes (N) of 32 pixels, the resulting expected standard deviation based on Eq. 1 is about 0.01 pixels. This value is both smaller than the accuracy generally admitted for such techniques and smaller than the ground measurements further presented. The formula of Eq.1 should be seen as an estimator of an upper boundary of the performance rather than an actual accuracy estimator.

In a first step, all the images of each time serie (ascending and descending) were co-registered on the first (reference) image of each series using a two degrees polynomial adjustment model derived from local correlation estimations. This procedure allows correcting the global shifts between the images that can be due to slight differences in the acquisition conditions. Then, the local offsets can be estimated using smaller windows (32 pixels in our case) and on denser grids (spacing of 16 pixels).

Considering the low values of the selected perpendicular baselines (between 1 m and 200 m) and the rather high displacement rate (~ 1 m.month-1), it is assumed that the range offsets due to local topography can be neglected with respect to ground displacement. In addition, stacking (as carried out) of offset maps obtained with different values of perpendicular baselines should partially compensate this topographic bias as it averages topographic components resulting from baselines with different signs and absolute values: we can suppose that with a large data set, the mean of the

perpendicular baselines associated to the different offset maps should much smaller than the maximal value (e.g. 200m in our case).

Multi-temporal processing:

The multi-temporal approach used for obtaining the evolution of the deformation is based on algorithms initially designed for deriving interferometric Time Series from a set of differential unwrapped interferograms (Berardino et al., 2002; Usai, 2003; Le Mouelic et al., 2005). Considering N differential interferograms (phase $[\Phi_i]$) obtained from M SAR images, the phase ($[\varphi_j]$) time series to be processed has to verify the following relation:

$$\begin{bmatrix} \Phi_1 \\ \Phi_2 \\ \Phi_3 \\ \dots \\ \Phi_N \end{bmatrix} = A \begin{bmatrix} \varphi_1 \\ \varphi_2 \\ \varphi_3 \\ \dots \\ \varphi_M \end{bmatrix} \quad (2)$$

where A is a matrix containing -1, 0 or 1 value according to the generated differential interferograms. Such over-determined linear system can be solved using a least-square solution. Once re-processed in Time Series (with respect to the first SAR acquisition), one can compute surface velocity maps on sub-intervals of the time-span covered by the SAR data set.

In SAR interferometry, the phase related to displacement rates can be obtained by linear regression of $[\varphi_j]$ with respect to the corresponding images acquisition dates on the whole image acquisition time-span or on shorter time intervals of interest.

For the present analysis, the previous algorithm was adapted to correlograms by replacing the phase ($[\Phi_i]$) values by pixel offsets values in the azimuth direction $[az_i]$ or in the range direction $[r_i]$. We thus derive times series of surface displacement in 2 directions. Once the azimuth and range time series are obtained, the deformation rates are calculated along range and azimuth over sub-period by linear regression. This methodology has been already applied on the C-band ENVISAT Advanced SAR (ASAR) data to a volcanic areas characterized by large deformation dynamics (Casu et al., 2011). Here, its applicability for HR X-band SAR monitoring of an active landslide is demonstrated.

A first estimate of the precision of the estimated displacement rates consists in dividing the offset standard deviation error by √N (where N is the number of independent offset maps) and by <ΔT>

(which is the average time span corresponding to the stacked offset maps). For example, in the ascending mode, only seven offset maps could be considered as independent (the other maps could be recomputed as linear combinations of these seven maps) with an average time span of 88 days. To convert the accuracy of individual correlograms (expressed in m) to displacement rates (expressed in $m.yr^{-1}$), we therefore multiply it by about 1.56. If we assume 0.1 m precision on offset estimates the resulting precision on the velocity would be about 15 $cm.yr^{-1}$.

3D displacement estimates

In order to produce 3D maps of the ground surface deformation, the combination of ascending and descending mode of observation is carried out based on the algorithm presented in de Michele et al. (2010). The basic idea is to retrieve the 3D deformation from four displacement rate components (1 azimuth and 1 LoS directions for the ascending and descending modes) obtained by the correlation computation for each point of the processing grid, affected by a certain quality (the SNR value associated with each offset measurement can be an indicator of the measurement precision). To construct the three component vectors representing the displacements, a least square formulation is proposed:

Let d be the vector constructed with the four measured values (e.g. two azimuth and two LoS components of the displacement rate) for a given point of the processing grid:

$$\mathbf{d} = \begin{pmatrix} az_{asc} \\ az_{desc} \\ los_{asc} \\ los_{desc} \end{pmatrix}$$

Let A, be a matrix containing the unitary vectors corresponding to the four directions along which the offsets are measured:

$$\mathbf{A} = \begin{pmatrix} u_{az-asc} \\ u_{az-desc} \\ u_{los-asc} \\ u_{los-desc} \end{pmatrix}$$

The three components displacement vector v is linked to d by:

$$\mathbf{d} = \mathbf{A}\,\mathbf{v} \quad (3)$$

The vector v can thus be derived from d by inverting Eq. 2 using a weighted (by the SNR values) least squares formulation. Considering both the unitary vectors used for the test site/sensor (and therefore the A matrix form) and the estimation of the standard deviation of the error on d resulting from Eq. 1, the standard deviation error on v derived from a pair of displacement rate maps (ascending and descending) is of the same order than the input rates.

The hypothesis behind this approach is that the 3D surface displacement rate that controls the measured pixel offsets is sufficiently similar among the epochs corresponding to the ascending and descending offsets maps to be merged. In an ideal situation, the ascending and descending time sampling should be identical (e.g. the same acquisition date), and displacement time series could be directly derived. In our case, the processing was performed with displacement rates that are less affected by time-span differences between correlograms and do not need rescaling.

Results: kinematic analysis of the La Valette landslide

Figures 2 presents the estimated 3D displacement map for the complete investigated period (April 2010 – November 2010). The map indicates that the most active part of the landslide is the upper part, and that the displacement rates decrease downslope. The maximum measured horizontal displacement rate is 14 $m.yr^{-1}$, while the maximum measured vertical velocity is 11 $m.yr^{-1}$.

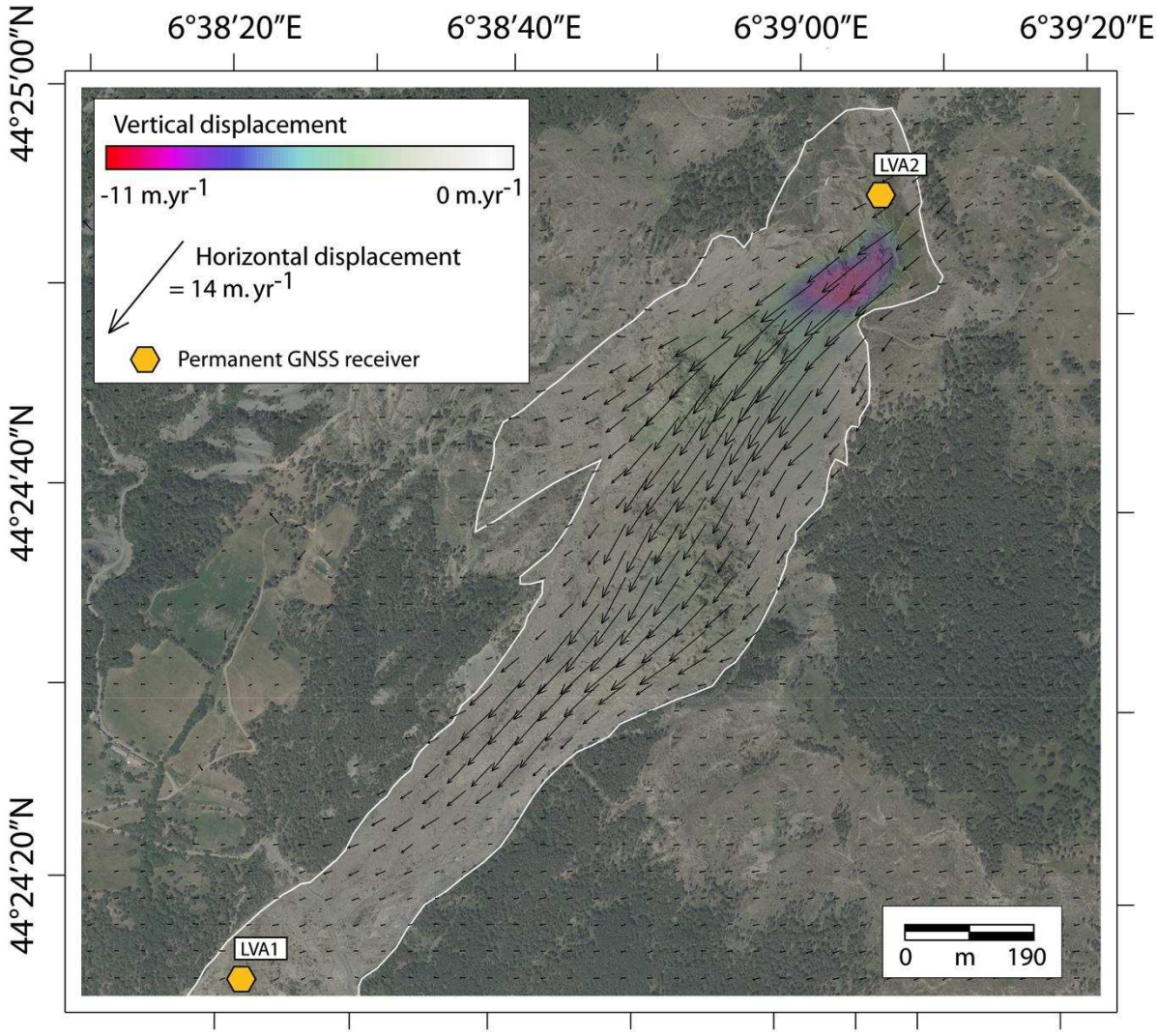

Figure 2: 3D displacement map of the La Valette landslide for the April–November 2010 period. Color represents the vertical displacements and arrows the horizontal displacements.

For identifying temporal variations in the behavior of the landslide, displacement rate maps were produced for three periods (April-June 2010, May-July 2010, July-November 2010; Fig. 3). We produced two maps for the period April-July, because it corresponds to the period of major potential changes in the kinematic regime. Noteworthy is the fact that – for this period - the offset estimation in descending mode is only based on three acquisitions for each sub-period. We can notice that the landslide displacement field is measured with high spatial details, and that spatial resolution of the results is fine enough to characterize the spatial variability of the displacement rates.

The three displacement rates maps show temporal changes in the velocity pattern, with higher displacements rates during the April-July period (up to about 20 $m.yr^{-1}$) and lower displacement rates

during the July-November period. Noteworthy, the upper part of the landslide seems to be globally affected by higher horizontal displacement rates between April and June 2010 than during the May-July period whereas the lower part seems to slightly accelerate between May and July.

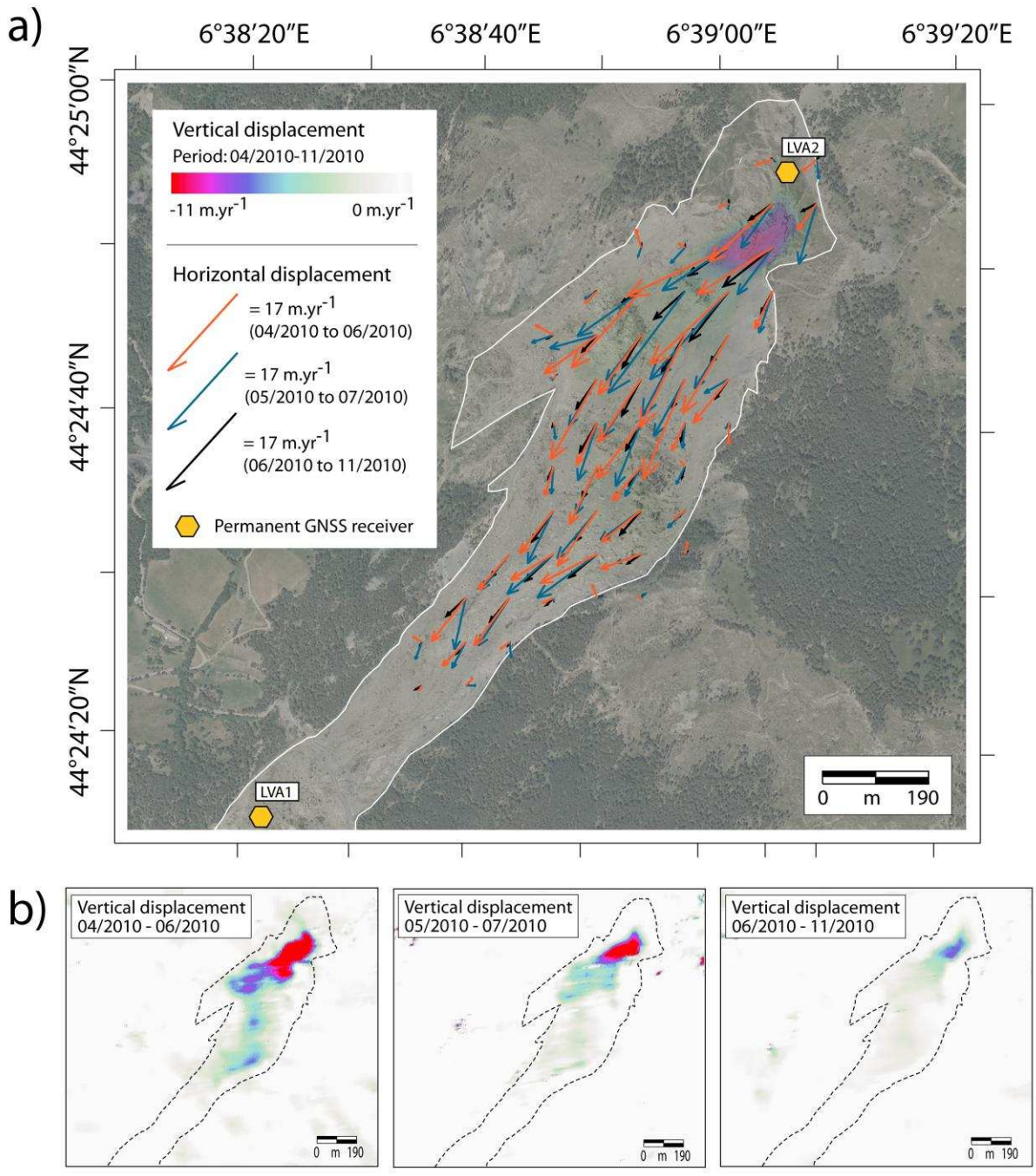

Figure 3: 3D displacement map on the La Valette landslide for the three sub-periods. a) Color represents the vertical displacements for the whole data set period, and arrows the horizontal displacement field per sub-period. b) vertical displacement for each period (same color scale).

We can notice that the descending mode data set covers a period of about five months longer than the ascending one. In the present analysis, this supplementary data was not used.

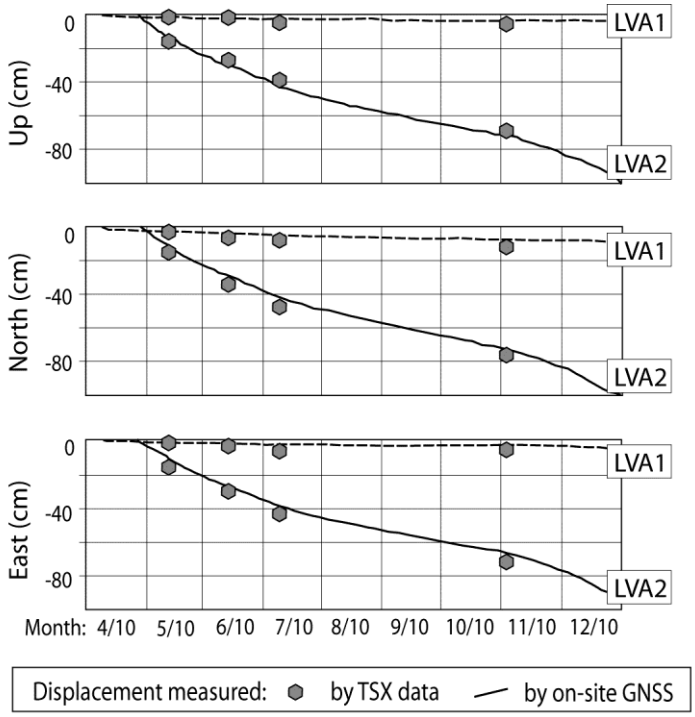

Figure 4: GNSS displacement time series at locations LVA1 (downslope) and LVA2 (upslope) for the period April-December 2010 and associated cumulated displacements measured in May, June, July and November 2010 by the TSX data for the three component of the displacement (Up, North, East). The displacements are cumulated from 8 April 2010 for the GNSS LVA1, and from 27 April 2010 for the GNSS LVA2.

Further, the accuracy of the displacement rates measured from the TSX data is quantified through a comparison (at the two locations LVA1 and LVA2; Figs. 2 & 3) with the displacements measured on-site by two permanent dual-frequency GNSS receivers (Trimble NetR9) of the French National Landslide Observatory OMIV (http://omiv.unistra.fr/). The GNSS observations (acquired at a frequency of 30s for 24h sessions) are processed daily using the GAMIT/GLOBK software. To compute the cumulated displacement from the TSX data based on maps at different time-spans but having time overlaps between them (e.g., for descending mode, time spans are t_0-t_3, t_1-t_5,t_4-t_7, where t_0,...,t_7 are the TSX acquisition dates on the full period of interest chronologically ordered. The periods t_1-t_3 and t_5-t_7, therefore correspond to overlaps. The following procedure has been used. The displacements are cumulated starting from the date of the first TSX image acquisition (e.g. t_0 is 8 April 2010). The

cumulated displacement at the starting date of the second time span is estimated using the velocity estimation of the first time span (e.g. for descending mode data, $d(t_1)=d(t_0)+V_0(t_1-t_0)$ where V_0 is the first velocity estimate). By iterating to the three displacement rate maps (and taking t_0 as reference date), we were able to compute four estimates of the cumulated displacement to be compared to the GNSS observations. Figure 4 presents the GNSS displacement time series obtained for the period April-December 2010 and the corresponding amount of cumulated displacement measured from the TSX data. For the three components (Up, North, East), the accuracy of the TSX displacements is in the range of ± 12 cm for the North and East components and ± 8 cm for the Up component in comparison to the GNSS cumulated displacements. The landslide kinematic pattern is therefore well identified by the TSX data.

Conclusions and perspectives

This work demonstrates the interest of sub-pixel image correlation techniques applied to series of HR X-band SAR images for mapping and quantifying landslide displacement patterns. The characteristics of these data in terms of spatial resolution, geometry, repetitiveness and low dependence to the weather conditions are very suitable for landslide monitoring. It appears as a performing alternative to optical HR image correlation whose data can be hampered by atmospheric conditions.

In the case of the La Valette landslide, the displacements observed for the period 2010-2011 are well depicted and are in agreement with the ground-based displacement observations. Displacement rates of up to 16 $m.yr^{-1}$ are mapped and changes in the kinematic regime are detected with a decrease of the displacement rates between the months of July to November.

The procedure for deriving such maps has revealed to be simple (and therefore easily automatable) and robust (no biases were detected during the processing). Noteworthy is the fact that the displacement rates are much higher than the expected accuracy with the reduced data set (seven images in ascending mode): in fact, the image acquisition was planned according to *a priori* knowledge on the foreseen displacement. Therefore, for landslides characterized by a different kinematic regime, a different data acquisition strategy should be used.

In particular, for faster landslides (with displacement rates of $m.month^{-1}$), the high repetitiveness of the current HR X-band space-borne sensors (TSX or Cosmo-Skymed) would allow to adjust (by increasing the acquisition rate) the inter-acquisition time span to higher displacement rates. As well,

the accuracy of the method is also sufficient for monitoring slower landslides (with displacement rates of dm.yr^{-1}) if longer time spans (e.g. years and more) are used. The proposed monitoring technique can therefore be applied to a wide range of landslide types.

Acknowledgements

The TerraSAR-X data used for this study was provided by DLR in the framework of the LAN0666 project. Processing was carried out in the framework of the project SafeLand "*Living with landslide risk in Europe: assessment, effects of global change, and risk management strategies*" (Grant Agreement No. 226479) funded by the 7th Framework Programme of the European Commission. The GNSS data are provided by the French Landslide Observatory (OMIV: Observatoire Multidisciplinaire des Instabilités de Versants: http://omiv.unistra.fr).

358

359

360 **References**

361 Bamler, R., & Eineder, M. (2005). Accuracy of differential shift estimation by correlation and split-
362 bandwidth interferometry for wideband and Delta-k SAR systems, *IEEE Geoscience and Remote*
363 *Sensing Letters, 2*, 151-155.

364 Berardino, P. Fornaro, G., Lanari R., & Sansosti, E. (2002), A New Algorithm for Surface Deformation
365 Monitoring Based on Small Baseline Differential SAR Interferograms, *IEEE transactions in*
366 *geoscience and remote sensing, 40(11),* 2375-2381

367 Casu, F., Manconi, A., Pepe, A., & Lanari R. (2011). Deformation time-series generation in areas
368 characterized by large displacement dynamics: the SAR amplitude Pixel-Offset SBAS technique,
369 *IEEE Transactions on Geoscience and Remote Sensing, 49(7)*, 2752-2763.

370 Colas, G., & Locat, J. (1993). Glissement et coulée de La Valette dans les Alpes-de-Haute-Provence.
371 Présentation générale et modélisation de la coulée. *Bulletin de Liaison des Laboratoires des Ponts*
372 *et Chaussées, 187*, 19–28

373 de Michele, M., Raucoules, D., de Sigoyer, J., Pubellier, M., & Chamot-Rooke, N. (2010). Three-
374 dimensional surface displacement of the 2008 May 12 Sichuan earthquake (China) derived from
375 Synthetic Aperture Radar: evidence for rupture on a blind thrust. *Geophysical Journal International*,
376 *183***,** 1097-1103.

377 Delacourt C., Allemand P., Casson B.,& Vadon H.(2004). Velocity field of the “La Clapière” landslide
378 measured by the correlation of aerial and QuickBird satellite images. *Geophysical Research*
379 *Letters*, 31(15), L15619

380 Delacourt, C., Raucoules, D., Le Mouelic, S., Carnec, C., Feurer, D., Allemand, P., & Cruchet M.
381 (2009). Observation of a large scale landslide in La Reunion Island using Differential SAR
382 interferometry (JERS and Radarsat) and correlation of optical images (Spot 5), *Sensors, 9(1)*, 616-
383 630.

384 Hibert, C., Grandjean, G., Bitri, A., Travelletti, J., & Malet, J.-P. (2011). Characterizing landslides
385 through geophysical data fusion: Example of the La Valette landslide (France*). Engineering*
386 *Geology, 128*, 23-29.

Le Mignon, G., & Cojean, R. (2002). Rôle de l'eau dans la mobilisation de glissements-coulées (Barcelonnette - France). *Proceedings of the 1st European Conference on Landslides,* Swets & Zeitlinger, Lisse, 239-245.

Le Mignon, G. (2004). *Analyse de scénarios de mouvements de versants de type glissement-coulées. Application à la région de Barcelonnette (Alpes-de-Haute-Provence, France)*. PhD Thesis, Paris: Ecole Nationale des Ponts et Chaussées.

Le Mouélic, S., Raucoules, D., Carnec, C., & King, C. (2005). A Least-squares adjustment of multi-temporal InSAR data – Application to the ground deformation of Paris, *Photogrammetric Engineering and Remote Sensing, 71(2)*, 197-204.

Leprince, S., Barbot, F., Ayoub, J., & Avouac, J.-P. (2007). Automatic and Precise Ortho-rectification, Coregistration, and Subpixel Correlation of Satellite Images, Application to Ground Deformation Measurements. *IEEE Transactions on Geoscience and Remote Sensing, 45(6)*, 1529-1558.

Mattar, K., & Gray, A, (2002). Reducing ionospheric electron density errors in satellite radar interferometry applications, *Canadian Journal of Remote Sensing, 28(4)*, 593–600.

Malet, J.-P., Déprez, A., Ulrich, P., & Masson, F. (2012) Continuous monitoring and near-real time processing of GPS observations for landslide analysis: a methodological framework *Engineering Geology*, *(submitted 21 p*)

Michel, R., & Avouac, J.-P. (2002). Deformation due to the 17 August 1999 Izmit, Turkey, earthquake measured from SPOT images, *Journal of Geophysical Research-Solid Earth, 107*, article number 2062.

Pathier, E., Fielding, E., Wright, T., Walker, B., Parsons, B., & Hensley S.(2006). Displacement field and slip distribution of the 2005 Kashmir earthquake from SAR imagery, *Geophysical Research Letters*, 33, L20310, doi:10.1029/2006GL027193.

Quegan, S., & Lamont J. (1986). Ionospheric and tropospheric effects on synthetic aperture radar performance, *International Journal of Remote Sensing, 7(4)*, 525–539.

Samyn, K., J. Travelletti, Bitri, A., Grandjean G., & Malet J.-P. (2012). Characterization of a landslide geometry using 3D seismic refraction traveltime tomography: The La Valette landslide case history, *Journal of Applied Geophysics, 86*, 120–132.

415 Scambos, T.A., Dutkiewicz, M.J., Wilsoni, J.-C., & Bindschadler, R.A. (1992(. Application of image
416 cross-correlation to the measurement of glacier velocity using satellite image data. – *Remote*
417 *Sensing of Environment, 42*, 177-186.
418 Squarzoni, C., Delacourt, C., & Allemand, P. (2003). Nine years of spatial and temporal evolution of
419 the La Valette landslide observed by SAR interferometry. *Engineering Geology*, *68(1-2)*, 53-66.
420 Travelletti, J., Delacourt, C., Allemand, P., Malet, J.-P., Schmittbuhl, J., Toussaint, R., & Bastard, M.
421 *(*2012a). A multi-temporal image correlation method to characterize landslide displacements with a
422 terrestrial camera. *International Journal of Photogrammetry & Remote-Sensing*, *70*, 39-55.
423 Travelletti, J., Malet, J.-P., Samyn, K., Grandjean, G., & Jaboyedoff, M. (2012b). Control of landslide
424 retrogression by discontinuities: evidences by the integration of airbone- and ground-based
425 geophysical information. *Landslides, in press* (DOI 10.1007/s10346-011-0310-8)
426 Usai, S. (2003). A Least Squares Database Approach for SAR interferometric data, Monitoring terrain
427 deformations at Phlegrean Fields with SAR interferometry. *IEEE Transactions on Geoscience and*
428 *Remote Sensing, 41*, 753–760.
429 Werner, C., U. Wegmuller, T. Strozzi, & A. Wiesmann (2005). Precision estimation of local offsets
430 between pairs of SAR SLCs and detected SAR images, *Proceedings of the Geoscience and*
431 *Remote Sensing Symposium (IGARSS)*, 25–29 July 2005, IEEE International Volume 7, 4803–
432 4805, 2005.
433 Wangensteen, B., Guomundsson, A., Eiken, T., Kääb, A., Farbrot, H. & Etzelmüller, B. (2006). Surface
434 displacements and surface estimates for creeping slope landforms in Northern and Eastern Iceland
435 using digital photogrammetry. *Geomorphology, 80(1-2)*, 59-79.
436 Yun, S., Zebker H., Segall P., Hooper A., & Poland M. (2007). Interferogram formation in the presence
437 of complex and large deformation. *Geophysical Research Letters*, *34*, L12305